Available online at www.sciencedirect.com
ScienceDirect
Icarus 190 (2007) 528–544
ICARUS
www.elsevier.com/locate/icarus

Analysis of a giant lightning storm on Saturn

G. Fischer [a,*], W.S. Kurth [a], U.A. Dyudina [b], M.L. Kaiser [c], P. Zarka [d], A. Lecacheux [d], A.P. Ingersoll [b], D.A. Gurnett [a]

[a] *Department of Physics and Astronomy, University of Iowa, 203 Van Allen Hall, Iowa City, IA 52242, USA*
[b] *150-21 Geological and Planetary Sciences, Caltech, Pasadena, CA 91125, USA*
[c] *NASA Goddard Space Flight Center, 8800 Greenbelt Road, Greenbelt, MD 20771, USA*
[d] *Observatoire de Paris-Meudon, 5 Place Jules Janssen, 92195 Meudon Cedex, France*

Received 13 November 2006; revised 27 March 2007

Available online 18 April 2007

Abstract

On January 23, 2006, the Cassini/RPWS (Radio and Plasma Wave Science) instrument detected a massive outbreak of SEDs (Saturn Electrostatic Discharges). The following SED storm lasted for about one month and consisted of 71 consecutive episodes. It exceeded all other previous SED observations by Cassini as well as by the Voyagers with regard to number and rate of detected events. At the same time astronomers at the Earth as well as Cassini/ISS (Imaging Science Subsystem) detected a distinctive bright atmospheric cloud feature at a latitude of 35° South, strongly confirming the current interpretation of SEDs being the radio signatures of lightning flashes in Saturn's atmosphere. In this paper we will analyze the main physical properties of this SED storm and of a single small SED storm from 2005. The giant SED storm of 2006 had maximum burst rates of 1 SED every 2 s, its episodes lasted for 5.5 h on average, and the episode's periodicity of about 10.66 h exactly matched the period of the ISS observed cloud feature. Using the low frequency cutoff of SED episodes we determined an ionospheric electron density around 10^4 cm^{-3} for the dawn side of Saturn.

Keywords: Saturn; Lightning; Saturn, atmosphere; Radio observations

1. Introduction

Saturn Electrostatic Discharges (SEDs) are impulsive short-duration radio bursts that were detected by the PRA (Planetary Radio Astronomy) instruments onboard both Voyagers (Warwick et al., 1981, 1982) as well as by Cassini/RPWS in the vicinity of Saturn (Gurnett et al., 2005; Fischer et al., 2006). Intrinsically, SEDs have a large frequency bandwidth, but in the PRA as well as in the RPWS time-frequency spectra the single bursts appear as narrow-banded short streaks due to the fact that they are detected only in the few channels being sampled in the frequency sweeping receiver during the short duration of the burst.

SEDs are generally organized in episodes with a duration of several hours occurring during consecutive Saturn rotations: They are recorded by the radio instrument when the supposed source is on the side of the planet facing the spacecraft, whereas no SEDs are detected when the source is below the radio horizon on the far side of Saturn. Table 1 shows all SED storms recorded so far by the Voyagers and Cassini indicating their identifying name, the time when they were recorded, the number of SEDs and episodes, plus the episode's recurrence period. Most of the SED storms in this table show a clear episodical on–off behavior. The recent giant SED storm E was such a storm with very distinct episodes occurring at each of 71 successive Saturn rotations, and there were no SEDs in-between the episodes. Only the SED storms V2 (Voyager 2, August 1981) and D (Cassini, June 2005) were not so clear in this respect with SEDs occurring also between episodes or episodes with a duration significantly longer than half a Saturn rotation, suggesting either a longitudinally extended source or more than one source at the same time.

* Corresponding author.
E-mail address: georg-fischer@uiowa.edu (G. Fischer).

0019-1035/$ – see front matter
doi:10.1016/j.icarus.2007.04.002

Table 1
Summary of all SED storms detected by radio instruments on Voyager (V1, V2) and Cassini (0 to E)

Name	Date	SEDs and episodes	Recurrence period
V1	Mid November 1980	18000 SEDs in 16(?) episodes	10 h 09 min (±6 min)
V2	End of August 1981	5000 SEDs in 10(?) episodes	10 h 00 min (±7 min)
0	End of May 2004	100 SEDs in 8 episodes	10 h 35 min (±6 min)
A	Mid July 2004	800 SEDs in 15 episodes	10 h 43 min (±2 min)
B	First half of August 2004	300 SEDs in 16 episodes	10 h 40 min (±2 min)
C	Throughout September 2004	4200 SEDs in 49 episodes	10 h 40 min (±1 min)
D	Mid June 2005	300 SEDs in 6 episodes	10 h 10 min(?) (±10 min)
E	January/February 2006	43400 SEDs in 71 episodes	10 h 39.8 min (±0.4 min)

Numbers were taken from Evans et al. (1981), Zarka and Pedersen (1983), and Fischer et al. (2006). Values for storm D (period is likely but questionable) and E are determined in this paper. The period for storm E was determined from DOY 25 to 49 (see Section 6). The numbers of episodes for V1 and V2 are not mentioned in the SED literature, Evans et al. (1981) display 16 episodes for V1 in their Fig. 2, and the value for V2 comes from looking at Fig. 4 in Zarka and Pedersen (1983), but there is no clear episodical on–off behavior for V2 episodes.

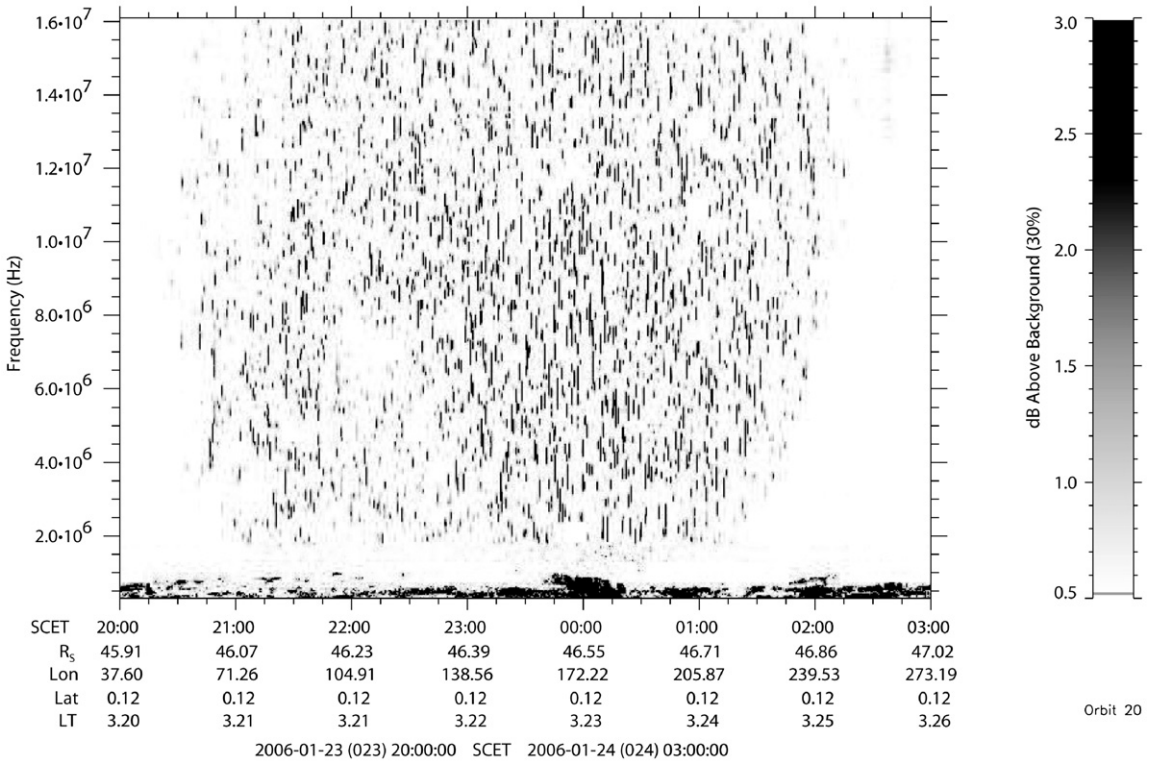

Fig. 1. Dynamic spectrum (intensity as function of time and frequency) over 7 h from 300 kHz to 16 MHz showing SED episode E2 from DOY 23/24, 2006. Orbital parameters of Cassini including distance in Saturn radii, sub-spacecraft western longitude, latitude, and local time are also indicated on the abscissa.

Fig. 1 shows the dynamic spectrum of the second episode of the giant SED storm from early 2006 with more than 4000 SEDs (the short vertical streaks), which is close to the number of all SEDs recorded during the whole storm C of September 2004. In contrast to the big SED storm E, the previous storm D from June 2005 consisted of just 6 episodes and lasted for about a week implying that SEDs did not show up during each rotation of Saturn. No other SED activity could be detected during the remainder of 2005, so there was a time gap of more than 8 months between storm C from September 2004 to the June 2005 storm, and a gap of 7 months to the next SED storm E in early 2006. No other SED activity besides storm E was detected by RPWS in 2006.

In this paper we will present the temporal occurrence of storms D and E, look at the duration of episodes and single bursts, and determine the burst rates and episode recurrence periods. First, there is a very brief description of the instrument and the data analysis method. Furthermore, we will show the intensity distributions of some SED episodes and we will look at the low frequency cutoff of SED episodes which shows an interesting behavior (see also Fig. 1) due to different viewing angles and ionospheric conditions. In the discussion we will emphasize that SEDs are the radio signatures of lightning from atmospheric storms at Saturn, which is supported by the images of cloud features provided by Cassini ISS (Imaging Science Subsystem).

We would like to mention the role that amateur astronomers on Earth played in the first days of the "giant" storm early 2006. They were the ones who realized the cloud as a sudden new feature and provided us images showing the location of the storm in agreement with the SED occurrence (see also acknowledgment). Their input helped locating the storm in the ISS images, which were taken a few days later. These ISS observations are presented in the companion paper by Dyudina et al. (2007), where a storm at the latitude of 35° South exhibits a small westward drift from about 170° to 185° Western longitude throughout the SED storm E.

2. RPWS instrument and data analysis method

The RPWS antenna system for the measurement of electric fields consists of three electric monopole antennas E_u, E_v, E_w of 10 m in length, and the monopoles E_u and E_v can be combined to form the dipole E_x. A detailed description of the RPWS (Radio and Plasma Wave Science) instrument onboard Cassini is given by Gurnett et al. (2004). For SED detection the HF1 and HF2 bands of the HFR (High Frequency Receiver) of the RPWS are used covering the frequency range of 325 kHz to 16 MHz. In both bands the receiver acts as sweeping receiver with a bandwidth of 25 kHz, and it can be programmed to use different frequency step sizes and integration times.

During both storms D and E the HFR was in the same mode: HF1 was performing a sweep from 325 to 1800 kHz with 60 frequency steps of a step size of 25 kHz. Within the 25 kHz passband there were 2 linear channels allowing a frequency resolution of 12.5 kHz. The integration time in HF1 was 80 ms and the instrument was in the so-called polarimeter mode, where both the autocorrelations of the E_x dipole and the E_w monopole as well as the crosscorrelation between them were measured. In case the direction of the incoming wave is known, the polarimeter mode allows a determination of the Stokes parameters describing the polarization state of the wave. During storm D only a few bursts were recorded in HF1, whereas during the big storm E more than 1600 SEDs were measured in this polarimeter mode. A polarization analysis of these events will not be done here, but will be the subject of a future paper.

HF2 was performing a sweep from 1825 to 16,025 kHz with 143 frequency steps with a step size of 100 kHz. The nominal integration time in HF2 was 40 ms, and only the autocorrelation of the dipole E_x was measured. For most of the time one sweep through HF1 and HF2 was performed every 16 s. Occasionally, during storm E, the instrument made one sweep every 8 s, and for this mode the integration time of HF1 was set to 40 ms and HF2 performed 72 frequency steps with a step size of 200 kHz, but all other parameters remained the same as with the 16 s sweep. We note that for calculating true flash rates, we have to take into account only the time when the receiver is actually "listening" at the SED frequencies. This duty cycle can be estimated by looking at how long the receiver dwells in HF2 with regard to the duration of a full sweep. For the used mode this is 5.034 of a 16 s sweep (or 2.5 of 8 s) resulting in a duty cycle of ∼0.31.

The data analysis method has already been described in detail by Fischer et al. (2006). Briefly, however, the intensity of an "SED pixel" (at a certain frequency and instant of time) has to be a certain threshold above the background intensity and above the intensity of the two neighboring pixels (at the same frequency but at the sweeps before and afterwards). Often an SED extends over more than one pixel in frequency because of the burst duration, and we call these multiple-pixel SEDs. For example, the 1600 SEDs recorded in HF1 during storm E, in fact, consist of more than 3000 SED pixels. The most important parameter for the extraction of the SED pixels from the RPWS data is the intensity threshold, which has to be set in accordance with the fluctuation σ of the background. This fluctuation depends on certain receiver and antenna characteristics, such as the integration time. It has been shown by Fischer et al. (2006) that a threshold of 4σ is an appropriate value for typical HFR measurements. By calculating this fluctuation in HF1 as well as in HF2 we have found the appropriate thresholds of 1.6 and 0.8 dB, respectively.

Our final list of SEDs was also cleaned of other kinds of radio emissions like solar bursts, jovian decametric arcs, or spacecraft interference, that were erroneously identified as SED pixels by the simple algorithm described above. Especially, some channels in HF1 (mainly harmonics of 100 kHz, and sometimes 1181, 1344, 1531, and 1756 kHz) were very noisy and had to be eliminated. Saturn Kilometric Radiation (SKR) is also detected in the lower part of the HF1 band, and we will show in Section 8 that the lower frequency cutoff of storm E SED episodes briefly extended down to SKR frequencies.

3. Occurrence of storm E episodes

Fig. 2 shows the number of detected SEDs per hour as a function of time for storm E. This storm consisted of 71 episodes (named E1 to E71) and lasted from January 23 (DOY 23) to February 23 (DOY 54), 2006. Altogether, 43,359 SEDs consisting of 83,311 pixels were recorded. The mean SED intensity was 2.5 dB above the galactic background, whereas the mean SED pixel intensity was 3.0 dB above the galactic background. The difference between mean SED intensity and mean SED pixel intensity is that for the former we first average over all SED pixels of each SED before calculating the mean intensity of all SEDs, whereas for the latter we just average over all SED pixel intensities. In Tables 2 and 3 we always calculate the mean SED intensity of each episode. SEDs in storm E occurred in each of the 71 successive Saturn rotations, but the number of SEDs per episode showed a large range, extending from just 3 SEDs for episode E38 up to 4081 for episode E2. The storm started with a massive outbreak of more than 2000 bursts in the first episode E1 and flash rates remained relatively high for the next 4 days as can be seen in Fig. 2. After periods of moderate and low SED activity the storm nearly returned to its original activity level about one week before it finally stopped. Fig. 1 shows a dynamic spectrum over 7 h of episode E2 with 4081 SEDs, which was the episode with the most SEDs recorded by Cassini to date. Tables 2 and 3 give a detailed listing of all storm E episodes with their main characteristics including center time

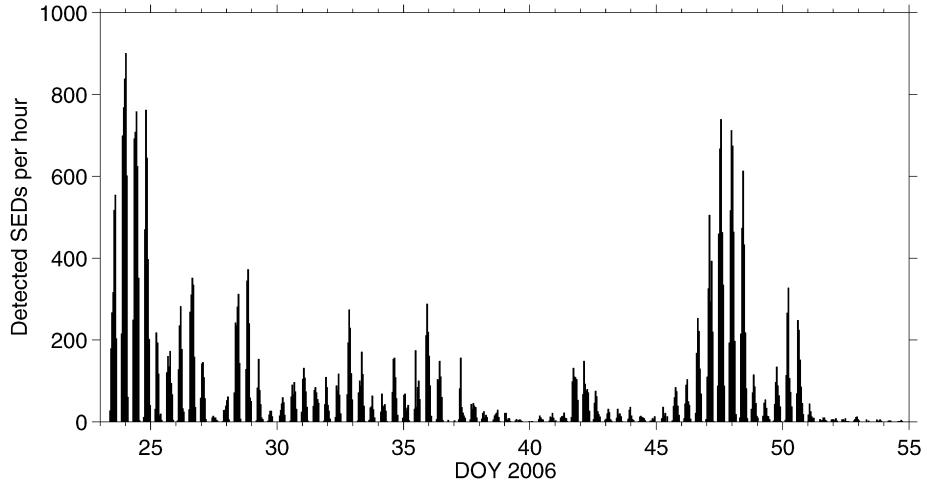

Fig. 2. Number of recorded SEDs per hour as a function of time for storm E in early 2006.

of occurrence (mean time of all SEDs of one episode), duration, number of SEDs (total and in HF1), true flash rate (taking into account the duty cycle of the instrument), and mean intensity. Also included are the distance to Saturn's 1-bar-level, local time, and the sub-spacecraft western longitude of Cassini at the center time during the respective episode.

During the course of storm E the Cassini spacecraft was first moving outbound from about 43 R_S (distance in Saturn radii from Saturn's 1-bar-level) and 3.1 h LT (local time) at episode E1 to apoapsis at 67 R_S and 4.8 LT around E31 (end of Cassini orbit 20). Then it moved inbound (orbit 21) and the SEDs ended when Cassini was at 19 R_S and 8.4 LT. Unluckily, no more SEDs occurred during the next periapsis, which was reached only about two days after the final episode E71. A plot of Cassini's orbit during storm E from early 2006 (as well as during storm D from June 2005) can be seen in Fig. 3 including asterisks indicating the position of Cassini at the center times of each SED episode. During storm E Cassini was practically in the equatorial plane of Saturn and the latitude changed gradually from only 0.13° at E1 to −0.33° at E71.

RPWS data coverage of SED storm E is nearly continuous except there are data gaps of several hours on DOY 36 and early 37 as well as late DOY 44 and early 45 during SED episodes E31 and E49, respectively. During E31 RPWS has data for only about 7 min from 18:18 to 18:25 SCET, DOY 36, and 4 bursts were detected in this time interval, and later there is data coverage from 00:00 to 00:35 SCET, DOY 37, when 3 more bursts were recorded giving a total of 7 SEDs for E31. There is also uncertainty about the end of episode E49 as data coverage ended before the episode seemed to be finished, and this is the reason why we put question marks in the episode duration column in Table 2 for E31 and E49. Occasionally there were a few more data gaps of a few tens of minutes during 6 other SED episodes (E5, E17, E40, E42, E50, E66).

4. Duration of SED episodes

Fig. 4 shows a histogram of episode durations with bins of half an hour of all SED episodes recorded so far by Cassini. It can be clearly seen that storm E episodes (dark gray bars) from early 2006 have a duration around 6 h, which is considerably different from the 2005 storm (light gray bars) and from the 2004 storms (0, A, B, C, indicated by black line). 53 of the 71 storm E episodes have a duration exceeding 5 h 20 min corresponding to half a Saturn rotation (Voyager radio period), but all of them are shorter than 6 h 40 min, which is ∼63% of a Saturn rotation. Assuming a single atmospheric storm source which is not too extended longitudinally as indicated by the images (Dyudina et al., 2007), there has to be a mechanism which explains the additional 1 h 20 min (or 45°) an SED episode can exceed one half of a Saturn rotation. For storm C of September 2004 Zarka et al. (2006) proposed temporarily trapping of radio waves below the nightside ionosphere resulting in an extension of the radio horizon below the planetary limb. The same propagation effect could be present as well for storm E as Cassini was at a similar local time on the morning side. In their model Zarka et al. (2006) calculate overall ray deviations of 36°–72° corresponding to 0.1–0.2 Saturn rotations, and the effect should only take place on the nightside (from where the storm is emerging) but not on the dayside (where the storm is disappearing).

For storm E the mean episode duration was 5.5 h, whereas the SED episodes of 2004 (see Fig. 4) had a mean episode duration of less than 3 h. The latter was explained by Fischer et al. (2006) as most likely being due to ionospheric damping of the SED radio waves on the dayside, as the absorption coefficient for radio waves is proportional to the electron density. A remarkable cloud (nicknamed "dragon") observed by Cassini/ISS in September 2004 (Porco et al., 2005) and most likely the source of SED storm C, was still visible from the spacecraft although the corresponding SED episodes had already terminated. The ionospheric damping might as well be present for storm E, but as storm E is more intense than storm C (Cassini is closer), SEDs from storm E were recorded almost until the visible cloud disappeared below the dayside horizon. The mean intensity of storm C SEDs was just 1.6 dB above background (Fischer et al., 2006), whereas it was 2.5 dB for storm E. It will

Table 2
Characteristics of the first 50 episodes of storm E (E1–E50) from early 2006

Episode name	DOY center	Hour center [hh:mm]	Duration from–to [hours]	Number of SEDs (total)	Number of SEDs in HF1	True rate [per h]	Mean intensity [dB]	Mean distance [R_S]	Western long. [°] center	Mean LT [hours]
E1	23	13:15	09:36–15:55	2063	200	1054	3.54	43.802	170.3	3.14
E2	23	23:22	20:17–02:28	4081	357	2132	3.73	45.449	151.1	3.23
E3	24	10:03	07:08–13:11	3385	132	1804	2.47	47.096	150.6	3.31
E4	24	20:10	17:53–23:34	2527	95	1433	2.31	48.575	131.0	3.39
E5	25	06:23	04:40–10:06	597	3	434	2.02	49.995	115.1	3.46
E6	25	17:45	15:16–21:13	751	25	406	2.66	51.488	137.8	3.54
E7	26	04:17	01:59–07:33	879	27	510	2.21	52.799	132.9	3.61
E8	26	15:21	12:40–18:27	1486	81	829	2.90	54.100	145.7	3.67
E9	27	01:27	23:09–04:46	516	32	297	2.50	55.222	125.9	3.73
E10	27	12:16	10:18–15:15	49	3	32	2.55	56.359	130.4	3.79
E11	27	23:58	20:59–02:20	215	3	130	2.36	57.515	164.8	3.86
E12	28	10:16	07:27–13:28	1291	87	692	2.24	58.471	152.0	3.91
E13	28	20:25	18:07–23:52	1192	35	669	2.04	59.359	133.9	3.96
E14	29	06:50	04:56–10:12	374	4	229	2.14	60.215	124.9	4.01
E15	29	17:50	15:51–19:27	84	14	75	2.70	61.058	134.3	4.06
E16	30	05:11	02:10–07:35	209	17	124	2.02	61.871	158.3	4.12
E17	30	15:47	12:54–18:42	419	15	233	1.75	62.574	155.8	4.17
E18	31	01:58	23:37–05:04	477	26	282	2.18	63.199	139.1	4.21
E19	31	12:57	10:11–15:52	371	30	211	2.19	63.820	149.5	4.26
E20	31	23:12	20:53–02:37	310	6	174	1.83	64.351	135.4	4.30
E21	32	10:04	07:45–12:48	377	19	241	2.18	64.862	140.8	4.35
E22	32	20:49	18:07–23:57	934	18	516	1.97	65.319	144.3	4.39
E23	33	07:57	04:53–11:05	587	12	305	1.87	65.738	159.3	4.44
E24	33	18:08	15:34–20:59	178	4	106	1.62	66.075	142.8	4.48
E25	34	04:51	02:34–08:02	237	2	140	1.79	66.383	144.2	4.52
E26	34	15:27	13:03–18:43	562	3	320	2.06	66.640	141.8	4.56
E27	35	02:04	23:34–05:01	246	4	145	1.70	66.850	139.3	4.60
E28	35	12:58	10:42–15:43	479	5	308	1.80	67.018	147.2	4.64
E29	35	23:11	21:21–02:38	981	8	599	2.22	67.131	131.9	4.68
E30	36	10:22	07:42–13:29	531	29	297	2.46	67.205	149.0	4.73
E31	36	20:50	18:18?–00:15?	7	0	62	1.34	67.227	141.9	4.77
E32	37	06:43	04:46–10:51	323	2	171	1.94	67.208	115.1	4.81
E33	37	18:32	15:44–21:29	208	11	117	2.73	67.132	153.8	4.85
E34	38	04:58	02:26–07:55	90	1	53	1.96	67.018	144.6	4.89
E35	38	16:22	13:10–19:10	101	6	54	2.12	66.841	170.3	4.94
E36	39	01:57	00:07–05:15	63	2	40	2.70	66.651	133.2	4.97
E37	39	13:16	10:16–16:12	22	0	12	2.71	66.378	154.6	5.02
E38	40	01:00	23:08–02:18	3	0	3	1.75	66.038	190.5	5.06
E39	40	10:16	08:09–12:55	42	5	28	3.71	65.728	143.3	5.10
E40	40	21:06	18:43–00:08	58	3	38	2.73	65.321	146.3	5.15
E41	41	07:56	05:35–11:00	77	0	46	1.77	64.860	153.6	5.19
E42	41	18:41	15:22–21:48	614	6	316	2.06	64.353	156.2	5.24
E43	42	04:58	02:07–08:47	558	7	270	2.00	63.821	142.9	5.28
E44	42	15:11	12:48–18:51	244	5	130	2.13	63.245	127.5	5.32
E45	43	02:25	23:31–05:15	93	0	52	2.48	62.556	146.2	5.37
E46	43	12:32	10:29–15:22	91	0	60	2.52	61.886	127.3	5.42
E47	43	23:28	21:17–02:27	97	1	60	2.54	61.108	135.6	5.47
E48	44	10:25	07:57–13:28	59	1	34	2.63	60.269	144.9	5.52
E49	44	21:23	18:41–22:53?	31	0	24	2.32	59.369	154.8	5.57
E50	45	07:32	05:25–10:53	93	0	74	1.57	58.482	136.9	5.62

In successive columns we list the name of the episode, the day of year (DOY) and the hour of the center time of an episode (mean time of SEDs belonging to this episode), the start and stop time of the episode, the total number of SEDs of the respective episode, the number of SEDs found in HF1 (<1825 kHz) for this episode, the true SED burst rate in number of SEDs per hour, the mean intensity of these SEDs in dB above the background, the mean distance to the 1-bar-level of Saturn in Saturn radii [R_S], the sub-spacecraft western longitude at the center time of the episode, and the mean LT (local time) of Cassini at the respective episode.

be shown later that SED episodes are less intense near their beginning and end. The anomalous long duration of about 9 h 45 min of episode D1 from 2005 (see Fig. 4 or Table 3) could be explained by two or more longitudinally separated SED sources being present at the same time.

5. Duration of bursts and burst rates

Fig. 5 shows a comparison of the distributions of SED burst durations for storms C, D, and E using a logarithmic scale for the ordinate axis. We only took SEDs recorded in HF2 for this

Table 3
Continuation of Table 2 for the last 21 episodes of SED storm E (E51–E71) from early 2006 plus 6 episodes of storm D from June 2005 (D00, D0, and D1–D4)

Episode name	DOY center	Hour center [hh:mm]	Duration from–to [hours]	Number of SEDs (total)	Number of SEDs in HF1	True rate [per h]	Mean intensity [dB]	Mean distance [R_S]	Western long. [°] center	Mean LT [hours]
E51	45	18:40	15:45–21:52	313	6	165	2.24	57.446	152.1	5.68
E52	46	05:19	02:29–08:29	341	3	183	1.83	56.394	150.6	5.74
E53	46	16:03	13:12–19:01	861	10	477	2.01	55.267	152.8	5.80
E54	47	03:06	23:53–06:08	1853	28	955	2.30	54.038	165.0	5.86
E55	47	13:21	10:30–16:47	2836	33	1457	2.18	52.834	150.0	5.93
E56	47	23:59	21:06–03:19	2774	59	1439	2.46	51.514	148.2	6.00
E57	48	10:36	07:40–14:16	2051	60	1000	2.68	50.121	146.0	6.07
E58	48	20:50	18:29–00:19	371	8	205	2.77	48.708	130.3	6.14
E59	49	07:49	05:08–11:21	180	1	93	2.27	47.105	140.1	6.22
E60	49	18:49	15:56–22:02	465	17	246	2.58	45.407	150.5	6.31
E61	50	05:20	02:43–08:44	925	19	497	2.43	43.694	144.2	6.40
E62	50	15:39	13:22–19:39	840	7	431	2.74	41.917	131.7	6.50
E63	51	02:18	00:08–05:53	117	0	66	2.27	39.983	129.5	6.61
E64	51	14:27	11:23–17:07	39	0	22	2.77	37.635	177.8	6.75
E65	52	00:49	22:12–03:28	28	0	17	2.55	35.502	166.4	6.89
E66	52	10:35	08:18–14:22	25	1	14	3.43	33.377	133.8	7.03
E67	52	22:05	19:46–00:23	40	8	28	4.69	30.707	159.8	7.22
E68	53	08:08	07:19–09:59	7	0	8	4.86	28.215	136.1	7.42
E69	53	19:15	17:04–21:22	16	1	12	3.92	25.254	147.5	7.69
E70	54	05:31	04:14–06:15	7	0	11	4.62	22.305	129.7	7.99
E71	54	15:58	13:59–17:53	8	0	7	5.25	19.046	116.9	8.40
D00?	159	11:55	10:07–14:00	7	4	6	2.43	2.823	317.3	20.80
D0?	159	22:40	21:26–01:51	5	0	4	5.83	7.384	233.1	2.62
D1	160	07:43	03:06–12:51	128	0	42	5.46	11.354	160.2	3.87
D2	162	10:54	09:29–14:51	11	0	7	5.40	26.184	60.4	5.79
D3	164	05:41	02:29–08:57	123	8	61	4.98	33.324	56.4	6.41
D4	166	10:11	06:12–11:52	14	1	8	4.95	38.213	21.7	6.94

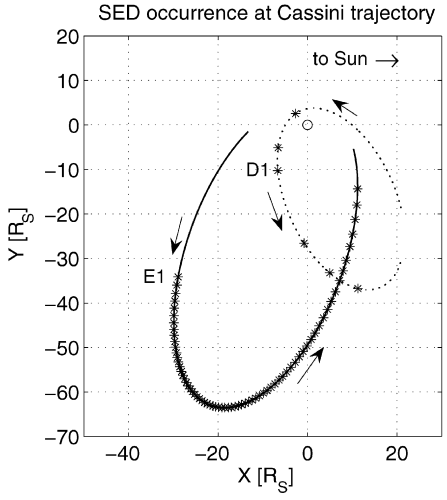

Fig. 3. Trajectory of Cassini during storm E (solid line, early 2006) and storm D (dotted line, June 2005) projected into the ecliptic plane of Saturn. The asterisks denote the positions of Cassini when SED episodes were recorded, and E1 and D1 denote the respective episode. Arrows indicate the direction to the sun as well as the counter-clockwise cruise of Cassini around Saturn when viewed from above the ecliptic plane. The positive x-axis points to the sun, and the negative y-axis in the direction of the movement of Saturn in its orbital plane.

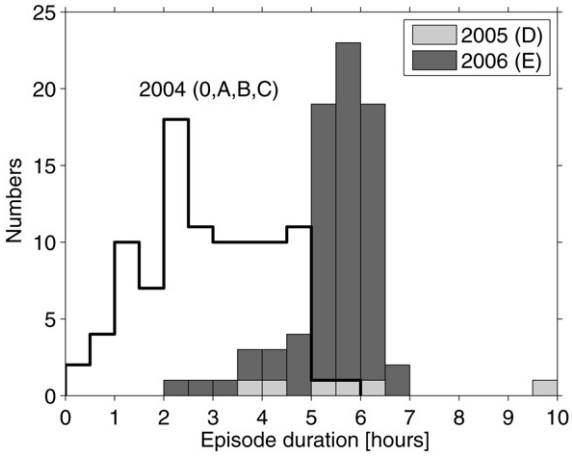

Fig. 4. Stacked bar-plot showing the durations of all SED storm E episodes from early 2006 (dark gray) and storm D episodes from June 2005 (light gray) in bins of half an hour. The line shows the distribution of the durations for all SED storms of 2004 (storms 0, A, B, C; compare to Fig. 7 of Fischer et al., 2006).

comparison, as practically no SEDs were recorded in HF1 for storm C and just a few for storm D; the integration time is different for HF1, and the interference at various frequencies of HF1 (mainly harmonics of 100 kHz) would also affect the analysis.

All SEDs in HF2 for storm C and D as well as storm E were recorded with a nominal integration time of 40 ms, which in practice is 35 ms for one-antenna measurements in HF2. The frequency settling time is already included here, giving burst durations that are multiples of 35 ms. Fig. 5 shows that the burst duration distribution can be well approximated by an exponential law: The exponential decrease of events with increasing

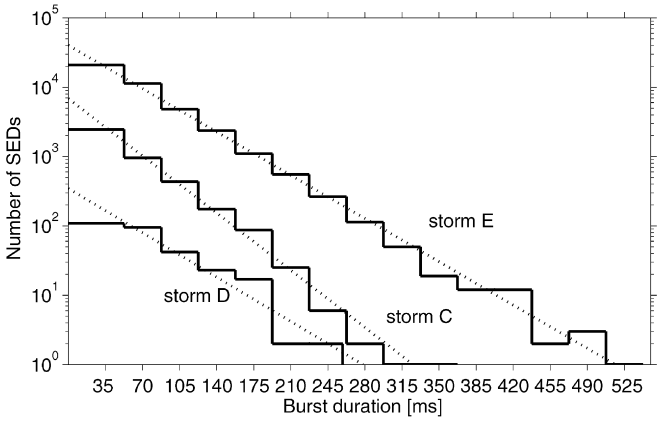

Fig. 5. Semi-logarithmic plot showing the distributions of SED burst durations for storm C (September 2004), storm D (June 2005), and storm E (early 2006), which were all recorded with a nominal integration time of $\Delta t = 40$ ms. The dotted lines represent best fits to the data assuming an exponential decrease of SED numbers with increasing burst duration.

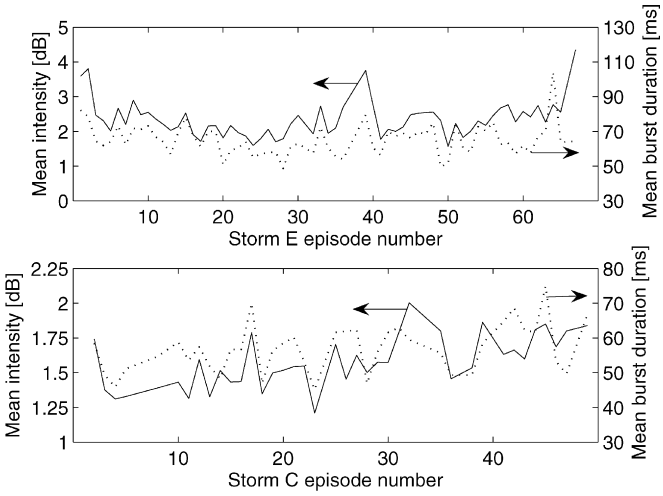

Fig. 6. Correlation between the mean intensity (solid lines, left y-axes, indicated by arrows) and the mean burst duration (dotted lines, right y-axes) of the episodes from storm E (upper panel) and C (lower panel). Intensities and burst durations are averaged for each episode; episodes with less than 25 SEDs were skipped.

burst duration is evident and translates into a negative slope of the dotted lines in the semi-logarithmic plot of Fig. 5, representing an e-folding time of (49 ± 3) ms for the case of storm E. The e-folding time for storm D is similar at (48 ± 12) ms, but due to the smaller number of SEDs the error is relatively large. Interestingly, this is longer than the e-folding time of (37 ± 3) ms found for storm C SEDs or the e-folding time of 41 ms found for the Voyager 1 SEDs (Zarka and Pedersen, 1983). (The e-folding time of 47 ms for storm C calculated by Fischer et al. (2006) is due to their incorrect use of the nominal integration time instead of the one actually used.)

About 59% of storm C SEDs were one-pixel events and the maximum duration was 350 ms (10 pixels), whereas for storm E only about 51% of SEDs consisted of only one pixel and the maximum duration was 525 ms (15 pixels). The reason for this difference is unknown, but it seems possible that different storms show slightly different time characteristics. It will be shown in the next paragraph that the burst rates of storm E were also extraordinary. However, one of the reasons for the longer durations might simply be the higher intensity of the storm E SEDs with regard to the galactic background. As Fig. 6 shows, there seems to be a correlation between the mean intensity and the mean duration of all SEDs of an episode. We calculated sample correlation coefficients between these two physical quantities and found 0.51 and 0.62 for storms E and C, respectively. (For this calculation and for Fig. 6 we left out all episodes with less than 25 SEDs, i.e. C1, C6, C7, C9, C32, C33, C36, C39, C47, C49, and E31, E38, and E68–E71.)

The burst rates determined for storm E exceeded all other previously measured rates by far. Tables 2 and 3 show the "true" burst rate for each episode, which showed a high variability and varied from a few bursts per hour up to the maximum of $\sim$2100 h^{-1} (about one SED every 2 s) recorded for episode E2 (see Fig. 1). True burst rates for each episode are calculated by dividing the number of SEDs by the episode duration, but taking into account data gaps and the duty cycle of the instrument, which is 31% as has been shown in Section 2. This duty cycle corresponds to the dwell time of the receiver in the HF2 band. But, for the estimation of the SED rates we have also included the 1600 SEDs detected in band HF1. We have not accounted for the fact that many SEDs in HF2 and especially in HF1 are undetected simply because they are below the ionospheric cut-off frequency.

The mean burst rate for storm E was 367 h^{-1}, as 43,359 SEDs were recorded in about 381 h with a duty cycle of 31%. In 2004 the mean true SED burst rate was only 64 h^{-1} and the maximum reached in episode A1 was 322 h^{-1} (Fischer et al., 2006), both values being smaller by about a factor of 5 compared to the corresponding values of the extraordinary storm E. Zarka and Pedersen (1983) calculated the maximum occurrence of the SEDs around the closest approaches of Voyager 1 and 2. They found an emission rate of one SED for every 4 and 13 s (for V1 and V2, respectively), corresponding to burst rates of 900 and 277 h^{-1}, respectively. The maximum rate for storm E (at E2) is more than twice as high as the maximum Voyager rate, despite the fact that the former was measured at a distance of 45 R_S, whereas the latter was measured around Voyager 1 closest approach (CA), when the spacecraft was at a distance of just 2 R_S above Saturn's 1-bar-level. In case Cassini would have been at the Voyager 1 CA distance during SED episode E2, the SEDs would have been much more intense by about 27 dB. Additionally, a lot more SEDs would have been detected (for distributions of SED intensities see Section 7 and the figures therein), and the peak flash rate would have been some tens of SEDs per second, which would have probably saturated the receiver.

6. Periodicity of the SED storm E episodes

One of the most important characteristics of an SED storm is the recurrence period of its episodes. This period gives a clue about the latitude of the SED storm source, as Saturn's atmosphere has a banded structure and different latitudes (bands)

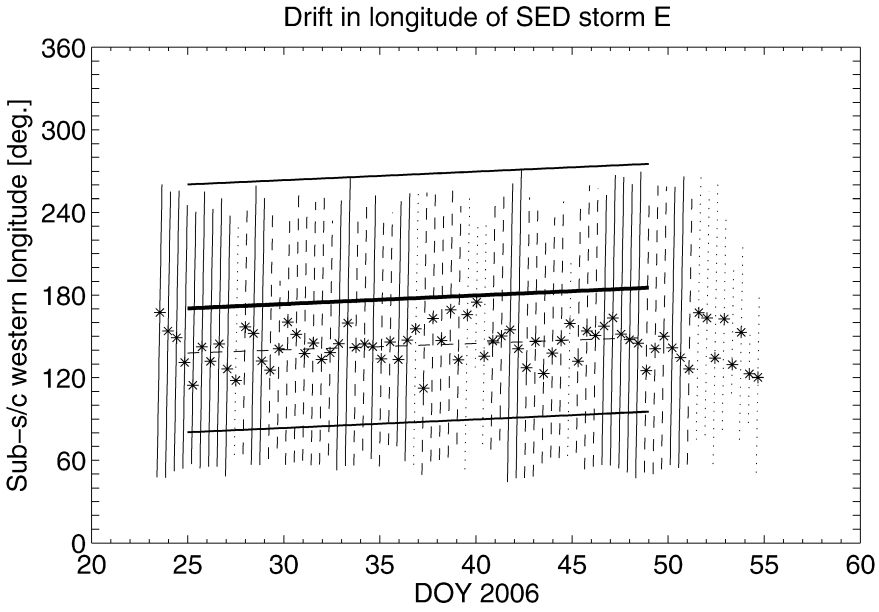

Fig. 7. Sub-spacecraft western longitude ranges (Voyager SLS) for the episodes of storm E from 2006 as a function of time. The asterisks denote the sub-spacecraft western longitude at the so-called center time, which is the mean time of all SED bursts within one episode. The nearly vertical lines indicate the longitude range from the first to the last SED of the respective episode. Dotted lines denote weak episodes with less than 50 bursts, dashed lines denote intermediate episodes with 50 to 500 bursts, and solid lines denote episodes with more than 500 SEDs. The nearly horizontal thick line indicates the interpolated position of the cloud feature as seen by Cassini/ISS, and the two thinner lines are parallel to the thick line and shifted by ±90 degrees. The dashed line represents the best fit of the drift for episodes E5–E60 (see text).

exhibit different wind speeds, and hence, rotation periods. For the Voyager SED storms the periods of 10 h 09 min (V1) and 10 h (V2) pointed to an equatorial source (see also Table 1), whereas the period of 10 h 40 min for storm C in September 2004 was consistent with a source in a zero wind velocity band (with regard to the Voyager radio period). The 2004 storm was detected by Cassini/ISS in such a band at a latitude of 35° South (Porco et al., 2005). Similarly, we will show in this section that the period of SED episodes of the 2006 storm derived from RPWS measurements is in perfect agreement with the period of the ISS observed cloud system (Dyudina et al., 2007).

Fig. 7 shows the drift in longitude of SED storm E in a very instructive way: The 71 nearly vertical lines (solid, dashed, and dotted corresponding to strong, intermediate, and weak SED episodes, respectively) denote the sub-spacecraft western longitude range from the time of the first to the last SED of each of the 71 episodes. The asterisks somewhere close to the middle of each episode represent the sub-spacecraft western longitudes at the center times. The thick line in the middle with a slightly positive slope corresponds to the actual location of the cloud as seen by observations of Cassini/ISS (Dyudina et al., 2007). The cloud resided at a western longitude of about 170° around DOY 25 and drifted westward and was observed at 185° around DOY 49, so there is a drift of about 15° in 24 days or ∼0.6° per day. Taking into account the planetocentric latitude of 35° South, this corresponds to a westward wind velocity of 6.0 m s^{-1} with regard to the Voyager SLS, and the period of the visible cloud is (10.665 ± 0.001) h (Dyudina et al., 2007). There are two parallel solid lines shifted by ±90° from the actual location of the storm (thick line) in Fig. 7, hence they represent the sub-spacecraft western longitude when the visible cloud rises above the eastern (left) horizon on the nightside and sets at the western (right) horizon on the dayside (for a relatively distant observer). It can be clearly seen that the SEDs start before the visible cloud can be imaged with the Cassini cameras, i.e. the radio horizon extends below the visible horizon on the nightside, which is possible by the ionospheric effect described by Zarka et al. (2006). On the other hand, this effect is not there on the dayside, and SEDs terminate either before the cloud has reached the visible horizon, or in the case of some strong SED episodes (like E6, E12, E23, E43, E54, E55, E57) the termination of the SED episode corresponds almost exactly to the time when the cloud is disappearing at the visible horizon. It can be also seen that the center time of an episode is reached before the cloud passes the central meridian at the sub-spacecraft position.

The center times help for the determination of the episode recurrence period, and a straight line fit can be performed in Fig. 7. We note that no correction for the LT change of Cassini during storm E is necessary in a plot of the sub-spacecraft western longitude as a function of time. A correction has only to be done when calculating the period in the time domain, whereas in Fig. 7 it is analogous to looking down from the spacecraft and “seeing” the storm at a certain western longitude. Performing a straight line fit to all 71 episodes, a slope corresponding to a period of (10.658 ± 0.005) h is obtained. We also performed a fit with a limited number of episodes: We omitted the first 4 episodes as there are no corresponding ISS observations available. We also left out the last 11 episodes for the same reason, and also because the last 8 episodes have less than 50 SEDs, making the center times less reliable. Fitting SED episodes E5–E60 a slightly positive slope of about 0.47° per (Earth) day is

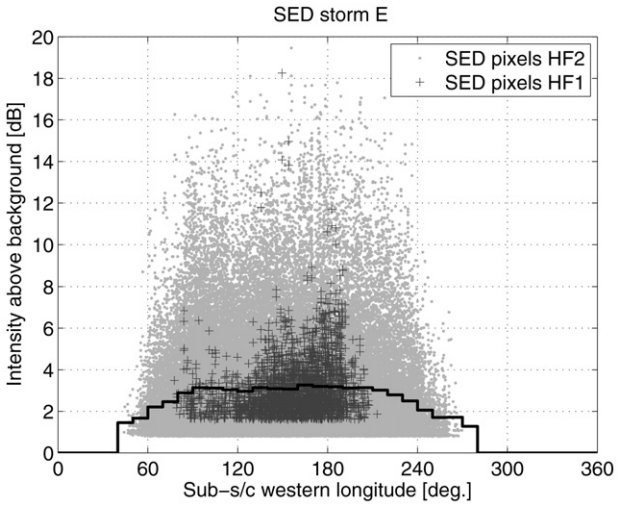

Fig. 8. SED intensities as a function of sub-spacecraft western longitude for storm E. SEDs from HF2 (⩾1.825 MHz) are plotted as light gray points, SEDs from HF1 (<1.825 MHz) are plotted as darker gray crosses over the light gray points. The black line indicates the average intensity in 10° longitude bins (for both HF1 and HF2 SED pixels).

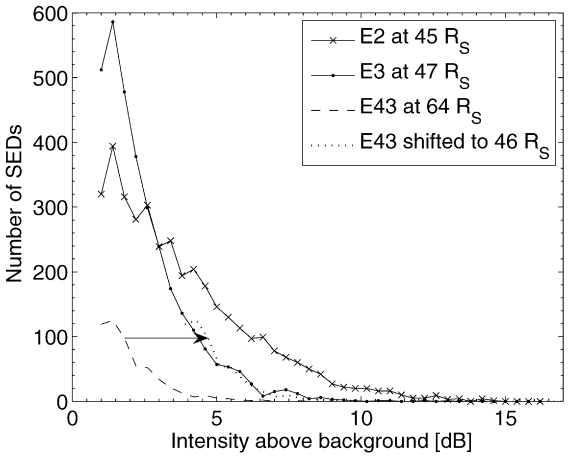

Fig. 9. Intensity distributions of SED episodes E2, E3, and E43: The number of SEDs (from HF2 band only) is plotted versus the intensity in dB above background in bins of 0.4 dB. E43 is also drawn as it would have been observed at a closer distance (shift by 2.9 dB to the right indicated by arrow).

calculated, and the fitted line can be seen in Fig. 7 as the dashed line close to the asterisks. The slope corresponds to a period of (10.662 ± 0.006) h (2σ confidence level), which is in excellent agreement with the period of 10.665 h determined from ISS images. Hence, assuming an SED source at a latitude of 35° South, RPWS SED measurements provide a westward drift of this source with a velocity of about (3.9 ± 4.4) m s^{-1}.

7. Storm E SED intensities and their distribution

Fig. 8 shows the intensity of the SED pixels (for a multiple-pixel SED we plotted all pixels) as a function of sub-spacecraft western longitude. Many important characteristics of storm E can be seen in this plot. The SEDs occur only at a longitude range from about 45° to 270° (see also Fig. 7), and SEDs are less intense at the edges of the episode. The latter can be not only seen with the light gray points, but is also clearly indicated by the black line, which gives the mean SED pixel intensity in 10° longitude bins. Additionally, we have distinguished between SEDs from HF2 (⩾1.825 MHz, light gray points) and HF1 (<1.825 MHz, darker gray crosses). There are no HF2 SED pixels with an intensity smaller than 0.8 dB above the background and no HF1 SED pixels below 1.6 dB, which is due to the different detection thresholds for HF1 and HF2 as described in Section 2. The maximum intensities found for single SED pixels were 18.3 dB for HF1, and 19.5 dB for HF2. The HF1 SEDs occur in an even more limited longitude range, which goes from around 78° to 213° of sub-spacecraft western longitude. For both bands this limited longitude range plus the reduced intensity at the edges can be explained by a single SED point source whose radio waves are influenced by ionospheric effects. For the HF2 band edges the single SED source should be close to the horizon implying a longer path through the ionosphere where absorption effects take place reducing the SED intensity. For the HF1 band edges the ionosphere is crossed at an oblique angle, which eventually raises the cutoff frequency above the HF1 upper frequency limit of 1825 kHz. We will investigate the low frequency cutoff of SED episodes in detail in the next section.

Fig. 9 shows the distribution of HF2 intensities (in 0.4 dB bins starting at 0.8 dB above background) for 3 different SED episodes of storm E. E2 is plotted as a solid line with crosses, and it includes more than 3700 SEDs. This can be compared directly to the weaker episode E3 including about 3200 SEDs in HF2 (solid line with points), as both were recorded at approximately the same distance around 46 R_S. We have also plotted another episode, E43, which was recorded from a distance of 64 R_S, and as signal intensities are expected to decrease with distance squared, the intensities of E43 seen from a distance of 46 R_S (for comparison with E2 and E3) would be stronger by a factor of $(64/46)^2 \approx 1.94$. This corresponds to a shift by about 2.9 dB in intensity, and in Fig. 9 we have plotted the distribution of E43 as seen by Cassini at 64 R_S (dashed line) as well as how it would be seen from 46 R_S (dotted line), where it is very close to the distribution of E3. An observer at this closer distance would have recorded many more SEDs during E43 than Cassini actually did, because one can expect a similar rise of SED numbers with decreasing distance for E43. So, in the plot of numbers of SEDs versus time in Fig. 2 one has to keep in mind that the episodes in the middle of storm E are underestimated as Cassini was near apoapsis (see also Fig. 3).

The shapes of the intensity distributions of the episodes of storm E show a certain variability, but the shapes of E2 and E3 as drawn in Fig. 9 can be considered as typical: E2 looks as if it could be fitted by a straight line with a certain negative slope, whereas E3 and E43 have a nearly exponential decrease or they could be described by 2 or 3 straight lines with different negative slopes. We note that the decrease in numbers of the first bin (from 0.8–1.2 dB above background) is due to our detection algorithm, as low intensity SEDs not only have to be a certain threshold above the background, but also the same threshold above both of their neighboring pixels.

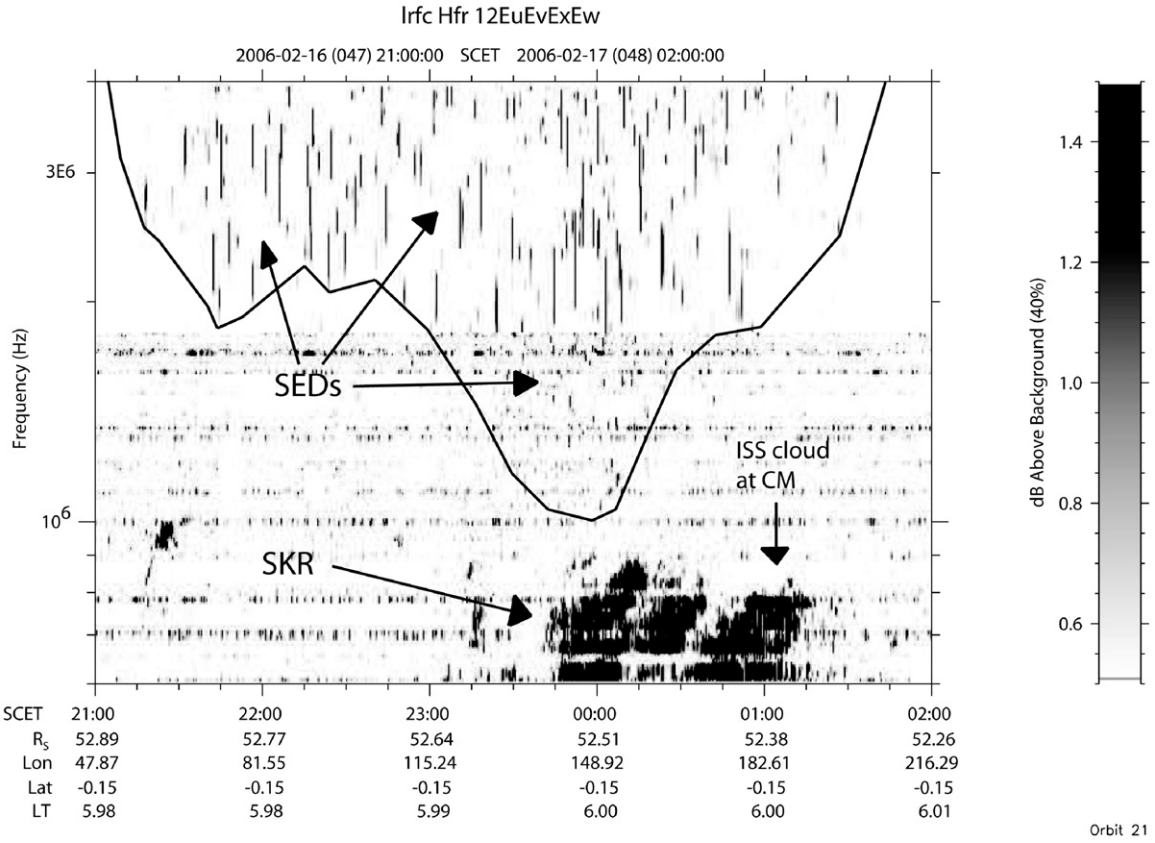

Fig. 10. Dynamic spectrum of SED episode E56 from DOY 47/48, 2006, with frequency going from 600 kHz to 4 MHz. Orbital parameters of Cassini are given like in Fig. 1. The line marks the lower frequency cutoff of this episode, and the vertically downward pointing arrow at 01:05 SCET indicates the time when the ISS observed cloud (SED source) is at the central meridian (CM).

8. The low frequency cutoff of SED episodes

The radio waves of SEDs can be seen as a natural signal probing Saturn's ionosphere. Hence, the low frequency cutoff of SED episodes provides information about maximum ionospheric electron plasma densities. The frequency minima of storm E episodes were in the range from about 770–2300 kHz in case of enough SEDs to see a clear minimum. The lowest HF1 frequency channel where SEDs occurred in storm E was at 768.75 kHz, and there were two SEDs with this frequency on DOY 23 during episode E1, the first one at 13:13 and the second one at 13:18 SCET.

The change of the lower cutoff frequency f_{cutoff} for the SEDs with time t (see spectra in Figs. 1 and 10) can be described by a simple equation, taking into account the angle of incidence $\alpha(t)$ between the zenith (normal to a horizontally stratified ionosphere) and the spacecraft as seen from the point where the radio wave leaves the ionosphere (which we approximate to be 2000 km above the ISS observed cloud system):

$$f_{\text{cutoff}}(t) = \frac{f_{\text{pe,max}}(t)}{\cos[\alpha(t)]} \quad \text{with } \alpha < 90^\circ, \tag{1}$$

where $f_{\text{pe,max}}$ is the maximum electron plasma frequency of the ionosphere very close to the position of the source. The distance from the source to the ionosphere is much less than the distance between the ionosphere and the spacecraft. This simple equation takes into account the non-normal wave incidence at the ionosphere for various positions of the storm with respect to the spacecraft.

Fig. 10 displays SED episode E56 with a logarithmic frequency scale as observed by Cassini at LT = 6.0. One can see clearly the noisier HF1 portion of the spectrum for frequencies below 1.825 MHz. The emission at the bottom of the spectrum is SKR (Saturn Kilometric Radiation). Additionally, the noise in HF1 also seems to vary with time, which is due to a rotation of the spacecraft causing a variation of antenna gain with time. Since the SEDs in HF1 are somewhat difficult to see in the spectrum, we have drawn a solid line around the whole SED episode in the time-frequency area, which gives the envelope of the low frequency cutoff (f_{cutoff}) of this particular SED episode. The minimum in frequency of E56 occurs at the HF1 frequency channel of 1043.75 kHz at 00:01 SCET (DOY 48), whereas in Fig. 10 we have indicated by an arrow the later time of 01:05 SCET when the storm cloud is at the central meridian as seen from Cassini. For the calculation of the plasma frequency $f_{\text{pe,max}}$ using Eq. (1) we first have to evaluate the angle of incidence α, which was done with the following geometrical parameters: at the time of E56 the SED source is at a longitude of $\lambda_{\text{storm}} = 185^\circ$ and a planetocentric latitude of $\phi_{\text{storm}} = -35^\circ$ as observed by Cassini ISS (Dyudina et al., 2007). Cassini is at a distance of 54.12 to 53.5 R_S at a practically constant planetocentric latitude of $\phi_{\text{Cas}} = -0.15^\circ$, and the western longitude changes from about $\lambda_{\text{Cas}} = 50^\circ$ to 260°. The calculated value

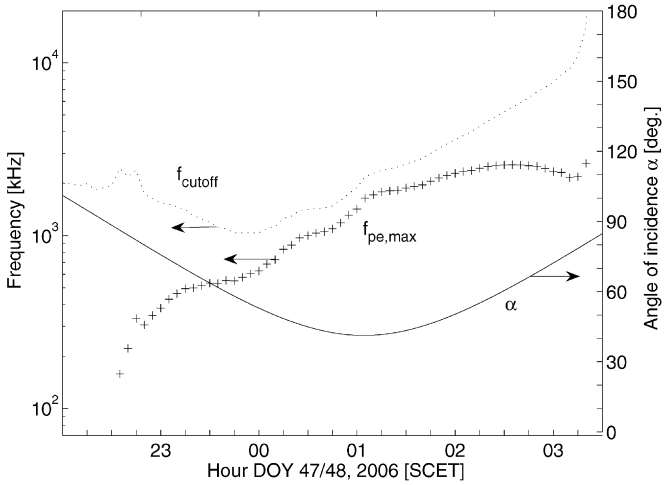

Fig. 11. Angle of incidence α (right ordinate, indicated by arrow), cutoff frequency f_{cutoff}, and derived maximum electron plasma frequency $f_{\text{pe,max}}$ (frequency axis on left side) as a function of time for SED episode E56 from DOY 47/48, 2006.

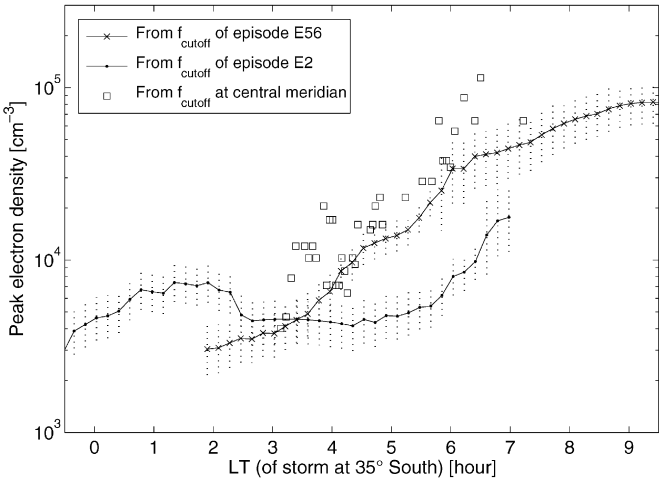

Fig. 12. Peak electron densities N_e of Saturn's ionosphere as a function of local time (of the SED storm) at a latitude of 35° South. N_e was derived from the lower frequency cutoffs of SED episodes E56 and E2 (lines with "x" and points, respectively), and from the lower frequency cutoff when the storm is at the central meridian seen from Cassini (squares). For E56 and E2 we have also drawn vertical error bars in a dotted line style, which were calculated by assuming an error of $\Delta\alpha = 2°$ for the angle of incidence and $\Delta f_{\text{cutoff}} = 100$ kHz for HF1 and $\Delta f_{\text{cutoff}} = 400$ kHz for HF2, respectively, for the error of the SED low frequency cutoff.

of α is plotted in Fig. 11 taking also the oblateness of Saturn into account. The radius vector from the center of Saturn to a planetocentric latitude of 35° South actually deviates from the normal to a horizontally stratified ionosphere by $\Delta\phi = 5.7°$, and this angle has to be added to the difference in planetocentric latitudes of Saturn and Cassini. The angle of incidence can also be well approximated by the formula

$$\alpha \approx \sqrt{\left(|\phi_{\text{storm}} - \phi_{\text{Cas}}| + \Delta\phi\right)^2 + (\lambda_{\text{storm}} - \lambda_{\text{Cas}})^2}, \tag{2}$$

as Cassini is much further from the center of Saturn than is the storm. As ϕ_{storm} and ϕ_{Cas} (and also λ_{storm}) are practically constant values, it is easy to see with the above formula that the minimum of α is reached when the storm's longitude equals the sub-spacecraft longitude (at 01:05 SCET), and then this minimum is given as the difference between the latitudes of the storm and Cassini including the correction $\Delta\phi$, which is ~41°. In Fig. 11 we have also plotted the cutoff frequency f_{cutoff} of episode E56 as well as the derived electron plasma frequency $f_{\text{pe,max}}$, both as a function of time with the frequency axis on the left side. It can be seen that the SEDs start before the cloud has arrived at the horizon, because $\alpha \geqslant 90°$ and then Eq. (1) cannot be used anymore. Generally, the closer α gets to 90°, the more $f_{\text{pe,max}}$ is in error, as ionospheric propagation effects like refraction become significant.

Finally, we calculate the peak electron density N_e from the maximum electron plasma frequency by inverting the equation $f_{\text{pe,max}}^2 = N_e e^2/(4\pi^2 m_e \varepsilon_0)$ with e as the elementary charge, m_e as the mass of one electron and ε_0 as the permittivity of free space. We now plot N_e not as a function of time but as a function of the local time of the storm in Fig. 12. The local time of the storm LT_{storm} as a function of time can be derived from the local time of Cassini LT_{Cas} and the respective longitudes of the storm and Cassini, λ_{storm} and λ_{Cas}, with the following equation:

$$LT_{\text{storm}} = LT_{\text{Cas}} + (\lambda_{\text{Cas}} - \lambda_{\text{storm}})\frac{1}{15°}, \tag{3}$$

where LT_{Cas} is given relative to Saturn's equatorial plane and not the ecliptic. In Fig. 12 we plot the electron densities from the lower cutoff frequencies of episodes E2 (line with points) and E56 (line with crosses). Also in Fig. 12 we plot the electron density derived from the cutoff frequency of various SED episodes (plotted as squares), when the SED source is at the central meridian. This occurs at the minimum of α, and the local time coverage from about 3 to 7 LT results from the LT change of Cassini during the course of storm E. The determination of the cutoff frequency at the central meridian was only possible at SED episodes with relatively high flash rates, and not all episodes could be used. The electron densities (derived in this way) are in reasonable agreement with the electron density profile determined from the whole low frequency cutoff of SED episode E56. The electron densities derived from E2 are slightly different, but this might be within the range of natural fluctuations. Both profiles from E2 and E56 show a rise in electron density with increasing local time. Cassini's local time at 3.2 LT during E2 allows us to determine electron densities at least to 0 LT. Generally, we have limited the density profiles for E2 and E56 to ~ ±4 h around the local time of Cassini. This corresponds to a range of $\alpha < 70°$, since for greater angles of incidence, the electron densities do not behave as expected due to ionospheric propagation effects. The electron density profile gained from E2 might be overestimated around 3–4 LT because SKR emissions might obscure some SEDs

We note the similarity between our profiles and the one determined by Kaiser et al. (1984) for the Voyager 1 SEDs, which were assumed to stem from an equatorial storm. Fig. 4 in Kaiser et al. (1984) shows an electron density of 10^5 cm^{-3} at 9 LT, which is in excellent agreement with our value. Our profile in Fig. 12 seems to be less steep, and an electron density of

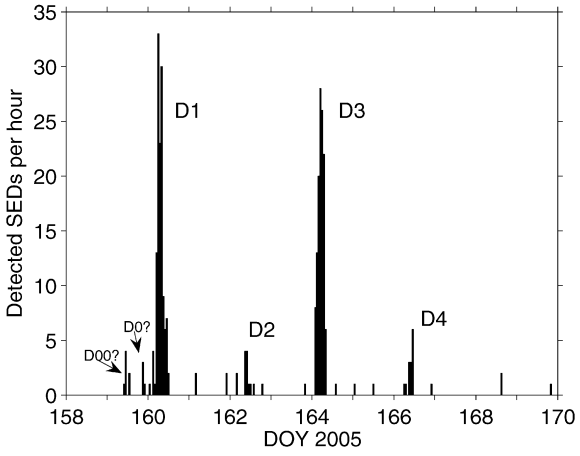

Fig. 13. Number of detected SEDs per hour for storm D from June 2005 as a function of time (DOY 2005). There are clearly 4 episodes D1 to D4, and there might be also two small precursor episodes named D00 and D0.

10^4 cm^{-3} is reached around 4.5 LT for E56, whereas Kaiser et al. (1984) reach the same value around 6 LT. But this is not surprising, as we have determined the electron density for a latitude of 35° South during Southern summer, where the Sun rises earlier and, hence, should start to increase the electron density before 6 LT, compared to the equatorial electron density determined near equinox by Kaiser et al. (1984). In fact, during the time of SED storm E in January/February 2006 the Sun was rising around 5.1 LT at a planetocentric latitude of 35° South at Saturn's 1-bar-level and even one hour earlier at 4.1 LT at a supposed ionospheric height of 2000 km.

9. The puzzling storm D

For completeness we briefly expand the description of storm D from June 2005 from that in Fischer et al. (2006). Fig. 13 shows the number of detected SEDs per hour as a function of DOY. There are four relatively clear episodes D1 to D4, and there are possibly two smaller precursor episodes, which were named D00 and D0 to avoid confusion with Fischer et al. (2006) and to indicate that they are very weak. Storm D started on June 8 (DOY 159) 2005 and the last SED was seen on June 2 18 (DOY 169), although the last episode D4 ended earlier on June 15 (DOY 166). Altogether, we identified 303 SEDs consisting of 646 SED pixels. At the bottom of Table 3 the most important characteristics of the storm D episodes can be found. The mean intensity of SEDs is 5.0 dB above the background, with a maximum intensity of nearly 14 dB (Fischer et al., 2006). The mean SED pixel intensity is 6.1 dB, and we found one pixel with a maximum intensity around 25 dB above background. These relatively high intensities are due to the fact that Cassini was close to Saturn when the SEDs were recorded, see the trajectory of Cassini during storm D in Fig. 3. The 7 SEDs of the precursor episode D00 were recorded when Cassini was on the late evening and night side of Saturn at a distance of ∼3 R_S. By the time of the second precursor episode D0 Cassini had moved to the early morning side to a distance around 7 R_S. The first intense episode D1 followed at the next Saturn rotation when Cassini was around 11 R_S, and the spacecraft moved further outbound to 38 R_S at D4 and to 39 R_S on DOY 169, when the last SED was recorded. The maximum burst duration of SEDs from storm D was 245 ms (7 pixel); see the burst duration distribution in Fig. 5.

There are some puzzling facts about storm D. The D1 episode lasted longer than 9 h, and the main episodes D1 to D4 seemed to occur with a periodicity of about 2 days (see Fig. 13). These things require further examination. Perhaps the best insight into storm D can be gained from Fig. 14. In this figure we have plotted the sub-spacecraft western longitudes as a function of time, for all of the storm D SEDs. We used 2 different point styles to distinguish between different SED intensities. We also labeled the names of the episodes, and with this plot it seems reasonable to see both D00 and D0 as bona fide episodes. There is one Saturn rotation between D00 and D0 as well as between D0 and D1; there are 5 rotations between D1 and D2, 4 between D2 and D3, and again 5 between D3 and D4. This is remarkably different compared to the highly regular storm E, which also varied in intensity, but appeared at every Saturn rotation. On the other hand, between some SED episodes in the year 2004 there were also time gaps of several Saturn rotations, and Fischer et al. (2006) concluded that there can be significant variability in SED activity within a time scale of a few hours. The durations of the SED episodes of storm D can be found in Table 3 as well as in Fig. 4. D1 lasts more than 9 h, assuming it extends from 11° to 328° longitude in the first half of DOY 160. But, Fig. 14 shows that there are gaps with no SEDs near the beginning and the end of this episode. D3 clearly lasts longer than 6 h, whereas the durations of the weak episodes D00, D0, D2, and D4, depend highly on our interpretation of which bursts are the first and the last ones for these episodes.

Remarkably, the last bursts of each episode except D2 seem to lie approximately on the straight dotted line which we have drawn in Fig. 14. In Section 6 we have calculated the period of storm E by using the center times of each episode (see Fig. 7), but in principle we could have done it similarly with the start or end times of the episodes. So, using the end times for storm D the slope of the dotted line in Fig. 14 is about one full rotation in 9.25 days (−38.9° per day) corresponding to a period of 10.17 h (10 h 10 min; estimated error ±10 min, at least). If this is the period of storm D, then an equatorial source is likely. The strange time gap of about two days between the major episodes D1–D4 might be just by chance, and there is no place in Saturn's atmosphere corresponding to this period. The characteristics of the bursts from storm D like intensity, burst duration, and especially the low frequency cutoff are like those of other SED storms. This leaves little doubt that also the storm D SEDs come from an atmospheric source below Saturn's ionosphere, and the 10 h 10 min periodicity seems a likely possibility.

Additionally, we have drawn short horizontal thick lines in Fig. 14 indicating the positions of possible minima in SED frequencies. We call them possible minima as they cannot be seen that clearly due to the low flash rates. Episode D1 and D3 seem to have 3 minima each, and the last minima of D1, D3, and D4

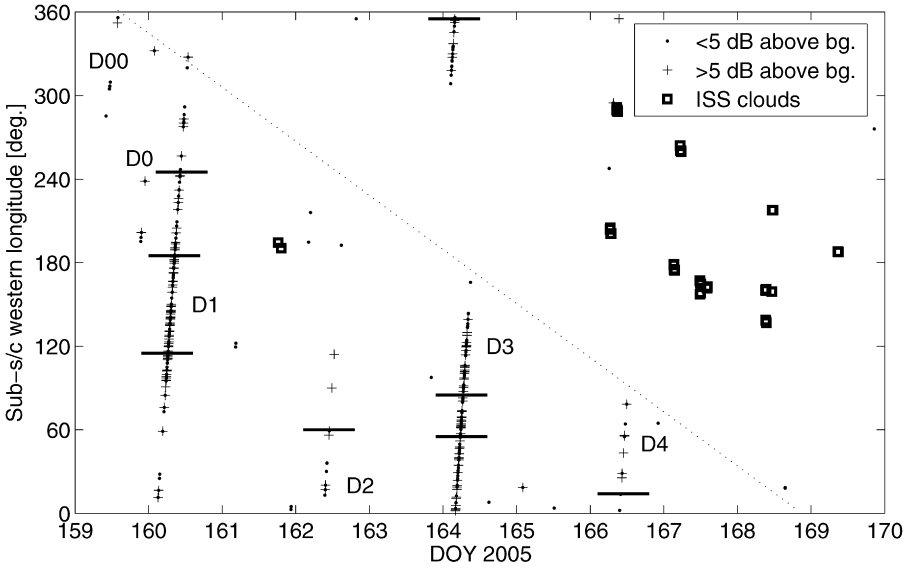

Fig. 14. Sub-spacecraft western longitude of storm D SEDs versus time. SEDs with different intensities (see legend) are plotted as dots or crosses, and ISS cloud observations are marked by bold printed squares. The short horizontal lines indicate the occurrence of a frequency minimum within one episode. The dotted line indicates a possible drift of storm D (see text).

lie approximately on a line which is nearly parallel to the dotted line indicating the end of the episodes. That means that the minima exhibit a similar drift as the episode ends, and the difference between the last minimum and the end of the episode seems to be a constant around 90° for D1, D3, and D4. These characteristics are consistent with a source disappearing at the horizon. For storm E episodes the frequency minima were normally obtained when the storm source passed under regions of low ionospheric electron density close to the sub-spacecraft longitude, and during D1 and D3 Cassini was at a local time of 3.8 and 6.4, respectively, very similar to storm E. Usually storm E episodes showed only one or sometimes two frequency minima. The existence of 3 minima for D1 and D3 suggests the possibility of two or even three longitudinally separated sources. Such a scenario could then easily explain the long duration of episode D1.

The ISS cameras have in fact detected three faint and sporadic clouds at Saturn's equator, which are marked by squares in Fig. 14. Image coverage is only limited (mainly after DOY 166, DOY 161 and early DOY 162), and the western longitude of the cloud seen around 180° on DOY 167 does not match the SED occurrence and might not be associated to the SEDs. Dyudina et al. (2007) have shown that the clouds at the "zero wind" velocity latitude of 35° South are due to fast eruptions, and subsequently, the plumes are sheared apart by the winds and fade with time. It might be that, due to strong vertical or latitudinal wind shear in the equatorial region, updrafting clouds are diluted and spread over a huge area, and, hence, cannot be clearly seen at all. This idea is supported by the fact that although the SED storm detected by the Voyager 1 radio instrument had a clear (equatorial) periodicity of 10 h 10 min (and was much stronger than storm D), no corresponding cloud observations by the Voyager cameras have been reported.

10. Discussion

The source of the SEDs was not always believed to be an atmospheric storm system. The Voyager 2 photopolarimeter detection of a narrow gap in Saturn's B ring at 1.81 R_S combined with the appropriate Keplerian revolution period of about 10 h 09 min led Evans et al. (1982) and Warwick et al. (1983) to conclude that this ring feature might be responsible for the SED bursts. Not only Evans himself published a paper one year later (Evans et al., 1983) questioning his own hypothesis, but also Burns et al. (1982, 1983) were more in favor for an atmospheric lightning storm source explanation. Kaiser et al. (1983) used an argument of visibility to say that SEDs should stem from an atmospheric source on Saturn. Zarka (1985a) analyzed and modeled the beaming, occurrence, episode drift, low frequency cutoff and absorption of the Voyager SEDs, which also considerably strengthened the evidence for an atmospheric source. A table showing the consistence of various SED properties with an atmospheric source and the inconsistencies and open questions related to a ring source can be found in Zarka (1985b). Nevertheless, some authors still questioned if SEDs are related to lightning discharges. For example, Majeed and McConnell (1996) suggested that SEDs may not be associated with atmospheric storm systems because the observed diurnal variation in peak electron densities deduced from SED measurements by Kaiser et al. (1984) did not match their ionospheric model. Also Rakov and Uman (2003) argue that due to the lack of optical and whistler observations, SEDs, alone, do not appear to be convincing evidence for saturnian lightning. We think that this situation has changed, now, with the correlated SED and convective cloud observations by Cassini RPWS and ISS, respectively, and we make strong arguments favoring the atmospheric source explanation in the following discussion. Ad-

ditionally, the observation of one whistler was recently reported by Akalin et al. (2006).

First, we will examine the ring source hypothesis again in the light of new Cassini observations and start with the main counter-argument of source visibility. The distance where the Keplerian velocity in Saturn's rings matches the Voyager radio period of about 10 h 40 min (and also the period of SED storms C and E) is 1.86 R_S (Esposito et al., 1984). For a relatively distant spacecraft a point source around 1.86 R_S would be visible for about 8.75 h, and would be obscured by Saturn by little less than 2 h. This is not much different for a source at 1.81 R_S, which has a period of 10 h 09 min. It should be seen for about 8.25 h with an occultation time of close to 2 h. Fig. 4 shows that not even a single SED episode observed by Cassini/RPWS has the typical duration an assumed source somewhere in the rings around 1.8 R_S should have. So, if the source is in the rings, it is tremendously difficult to explain why the vast majority of SED episodes are shorter than the geometric visibility would allow. The single exceptionally long episode D1 can be explained by longitudinally separated sources in Saturn's atmosphere. Warwick et al. (1983) assumed that a 200 m broad gap located at $(108{,}942 \pm 6)$ km from the center of Saturn is cleared by a small satellite, and that the SEDs would be caused by discharges between this negatively charged satellite and the positively charged outer edge of the gap. We note that the period of such a fixed "discharge" gap at 1.81 R_S is simply not consistent with the periods of SED storms 0, A, B, C, and E observed by Cassini. And, there are other examples of moonlets interacting with the rings; if this is a viable phenomenon, then there should be multiple SED sources in the rings at any given time, which is obviously inconsistent with the observed occurrence of SEDs.

Discharges in the rings would not only require an efficient electrification process, but also a mechanism for the separation of charges with different signs, and there is no consistent theory for how this could work. The Lorentz force can separate charged particles at exactly this radial distance, where the Keplerian orbital period equals the rotation period of the exterior magnetic field of Saturn. However, the latter has been determined by Giampieri et al. (2006) to be (10.785 ± 0.011) h, but no SED storm with this period has ever been observed up to now. Mendis et al. (1984) have described electrodynamic processes in the rings, and they also reviewed possible theories about the formation of the spokes, which first were thought to be possibly related to SEDs. Weinheimer and Few (1982) have critically evaluated some of these theories, and they note that the low conductivity of ice particles at the low temperatures in the rings would inhibit collisional charge transfer, a mechanism that is considered essential in the electrification of thunderclouds at Earth (Rakov and Uman, 2003). Further, no spokes were observed by Cassini until September 2005 (Mitchell et al., 2006), but there has been clearly SED activity before that (Fischer et al., 2006), so these two phenomena seem to be not related. One of the main arguments against an atmospheric storm explanation was the low frequency extension of the SEDs. In the Voyager era the frequency range of SEDs was observed to go from as low as 20 kHz up to the highest frequency of the PRA receiver of 40 MHz. However, it is rarely mentioned that the low frequency extension down to 20 kHz was a rather exceptional event which, in fact, occurred only at the episode around closest approach of Voyager 1. The frequency range from 3–1200 kHz at Saturn is dominated by Saturn Kilometric Radiation which can possibly obscure the SEDs. The SKR intensity and the lower and upper frequency limits of the SKR are highly variable, depending mainly on the rotational phase of Saturn and the solar wind conditions. Around the Voyager 1 closest approach the SKR remained within a frequency range of about 150–800 kHz, and about 30 bursts looking similar to SEDs could be identified below the SKR lower frequency boundary (Zarka and Pedersen, 1983). We reviewed these events visually on dynamic spectra and could confirm only those occurring from about 22:30 on November 12 to 01:30 SCET on Nov. 13, 1980, i.e. during the Voyager 1 closest approach episode. After 01:30 SCET on Nov. 13 the low frequency signals below 150 kHz appear to be due to intermittent SKR. Nevertheless, the point we want to make is, that no SEDs observed by RPWS in 2004 came close to SKR, and no SEDs below 1.3 MHz could be unambiguously identified (Fischer et al., 2006). Similarly, for storm D and E, the lowest frequency channels where SEDs were observed were 1068.75 and 768.75 kHz, respectively. Only a few episodes of storm E came close to the upper frequency boundary of SKR, as can be seen in Fig. 10, and we did not find any SEDs below the SKR.

The high flash rates of storm E provided a clear low frequency cutoff for many SED episodes, and as SEDs should be randomly distributed above this frequency cutoff, it is very unlikely that any bursts observed below this frequency cutoff are due to SEDs. They are much more likely due to SKR, jovian radio emissions, or other interference. So for all the more than 72,000 SEDs observed by the Voyagers as well as Cassini, the statement that the SEDs are below the SKR frequencies and go down to 20 kHz is, in fact, only true for maybe 30 of them or 0.04%. Nevertheless, these anomalous low frequency SEDs deserve further investigation and attention. Kaiser et al. (1984) noted that the low frequency events occurred only at the southernmost extremity of Voyager 1's closest approach (at latitudes between 23° and 39° South) between dusk and midnight. Connerney and Waite (1984) tried to explain these by invoking ionospheric holes caused by an enhanced influx of water at latitudes around 40° from the magnetically connected B-ring of Saturn. Perhaps future SED observations by Cassini at similar latitudes will shed some light on this problem.

Other effects, mainly related to the propagation of radio waves through the saturnian ionosphere, also need more detailed investigation. The extension of the radio horizon below the planetary limb when the SEDs occur on the nightside requires more detailed modeling. The clouds correlated with storms A, B, C, and E (Dyudina et al., 2007) have a small longitudinal extent of about 5°, so this "over horizon" effect should be present. Also, models of electron densities in Saturn's ionosphere (Moore et al., 2004; Mendillo et al., 2005; Majeed and McConnell, 1996) have difficulty explaining the night–day variation in electron density inferred from the Voy-

ager SED measurements (Kaiser et al., 1984). Section 8 of this paper confirms the Voyager results for the morning side of Saturn. The peak electron densities derived in this paper are in agreement with the peak electron density determined by the Voyager 2 egress radio occultation of about 10^4 cm^{-3} at the early morning side of Saturn's ionosphere near the planetographic latitude of 31° South (Lindal et al., 1985). On the other hand, recent Cassini radio occultations by Nagy et al. (2006) give peak electron densities only around 10^3 cm^{-3} around the equator at dawn, which they attribute to the difference in the solar cycle of Saturn between Voyager and Cassini observations. One point that has been neglected so far in ionospheric modeling, but which is essential for radio wave propagation, is the modeling of collision frequencies in Saturn's ionosphere. By including these we could draw conclusions about the attenuation of radio waves as a function of frequency for the edges of the episodes as shown in Fig. 8. Although there are still some points that need further explanations, the general shape of the low frequency cutoff of SED episodes with Cassini on the morning side of Saturn is consistent with an SED source moving from the nightside to the dayside under an ionosphere of increasing electron density, and one could not explain this shape with a source in the rings.

Finally, we come to the main arguments for a clear link between the SEDs and storm systems in Saturn's atmosphere. This has become possible by observations from RPWS together with ISS. The first results have been already published by Porco et al. (2005), and a comprehensive description can be found in the companion paper by Dyudina et al. (2007). For the 6 SED storms observed by RPWS, prominent cloud systems could be seen only at the planetocentric latitude of 35° South in the ISS images for 4 of them, namely the storms A, B, C, and E (see Table 1). For the two smaller storms 0 and D, no prominent clouds could by unambiguously identified. As latitude, phase, and drift for A and B are consistent with SED storm C, all three most likely stem from a single atmospheric storm system (Porco et al., 2005; Fischer et al., 2006). The occurrence of SEDs always matched the position and time when the storm was imaged on the near side of the planet (except for the "over horizon" SEDs). Additionally, the drift in longitude with time, is highly consistent between the images and the SED episodes. We have already presented the consistent periods derived from the images and the SED occurrence for storm E in Section 6. Dyudina et al. (2007) also show that there is a clear correlation between the brightness of the observed clouds and the number of SEDs for storms A, B, C, and E. Direct flashes of light were not observed on the nightside, which might be due to the depth of the lightning flashes within Saturn's atmosphere (Desch et al., 2006), the opacity of the clouds, or the brightness of the ring shine. On the dayside, different filters were used to image the clouds at different depths in the atmosphere. Using this technique, Dyudina et al. (2007) could see dense clouds reaching high altitudes suggesting updrafts. It is well known that terrestrial thunderstorms are characterized by relatively strong updrafts (Rakov and Uman, 2003), and updrafting water clouds on Saturn have been theoretically modeled by Hueso and Sánchez–Lavega (2004).

The January/February 2006 SED storm was "giant" in terms of the numbers of observed SEDs and burst rates. However, it might be possible that even greater lightning storms exist on Saturn. We can speculate that the SEDs observed by Voyager 2 in August 1981 were from the same storm as those observed by Voyager 1 in November 1980, about 9 month earlier. Similarly, strong lightning activity could be present during the rare major equatorial eruptions on Saturn as observed by the Hubble Space Telescope in 1990 (Westphal et al., 1992).

11. Conclusions

The giant lightning storm E of early 2006 provided a unique opportunity to study Saturn Electrostatic Discharges in great detail. It lasted for about one month and bursts appeared during each of the 71 consecutive Saturn rotations. In total, more than 43,000 SEDs were observed for this storm, and there were extraordinary high flash rates with a maximum of 1 SED every 2 s. The highly regular storm E episodes had a mean duration of 5 h 30 min, and a maximum duration of 6 h 40 min. The episodes generally ended before the difference between the storm source longitude and the central meridian of the spacecraft exceeded 90°, consistent with a source disappearing at the horizon. But, similar to the storm of September 2004, SEDs appeared about 0.1 planetary rotation before the visible cloud feature rose, which we attribute to an ionospheric radio propagation effect on Saturn's nightside. The SED bursts of storm E had durations ranging from 35 to 525 ms. The distribution of burst durations shows an exponential decrease with an e-folding time of (49 ± 3) ms. Taking into account the local time change of the spacecraft during storm E we determined the episode recurrence period from DOY 25 to DOY 49, 2006, to be (10.662 ± 0.006) h. This corresponds to a westward drift of a source at the planetocentric latitude of 35° South with a velocity of about (3.9 ± 4.4) m s^{-1} with respect to the Voyager rotation period, which is in excellent agreement with the westward drift of the observed cloud system in the images.

We examined the low frequency cutoffs of storm E episodes, which are consistent with a storm system emerging from the nightside and disappearing under the dayside ionosphere. Using the cutoff frequencies we determined the ionospheric electron densities at the storm latitude of 35° South from about 0–9.0 LT (typically 10^4 cm^{-3} at local dawn), which compare favorably to previous Voyager SED and radio occultation measurements.

We also examined the short SED storm D from June 2005 and outlined a possible scenario for it being an equatorial storm with a period around (10.17 ± 0.17) h and probably consisting of two or three longitudinally separated storm cells.

In the discussion we offered strong arguments that SEDs are the radio signatures of lightning flashes in Saturn's atmosphere. The SED storms episode durations, frequency extent, and shape of the lower frequency cutoff are inconsistent with a source in the rings. The main arguments for an atmospheric source are the correlated position of the convective cloud system and

the occurrence of SEDs, as well as their common recurrence period. Outstanding images of the cloud systems associated with the SEDs in the companion paper by Dyudina et al. (2007) provide evidence for updrafts in the clouds and show the correlation between cloud brightness and SED rates. Both of those are also effective arguments for an atmospheric lightning source.

Acknowledgments

The authors wish to thank Jean-Luc Dauvergne and Erick Bondoux from France, astronomers from the Association of Lunar and Planetary Observers, Jim Phillips from the USA, and Ralf Vandebergh from the Netherlands for sacrificing their sleep for science and performing telescope observations of Saturn during the night. We also thank the two anonymous reviewers for their suggestions.

The research at The University of Iowa was supported by the National Aeronautics and Space Administration through Contract 1279973 with the Jet Propulsion Laboratory.

References

Akalin, F., Gurnett, D.A., Averkamp, T.F., Persoon, A.M., Santolik, O., Kurth, W.S., Hospodarsky, G.B., 2006. First whistler observed in the magnetosphere of Saturn. Geophys. Res. Lett. 33, doi:10.1029/2006GL027019. L20107.

Burns, J.A., Durisen, R.H., Borucki, W.J., Showalter, M.R., Cuzzi, J.N., 1982. A comparison of Saturn's electrostatic discharges with lightning on various planets. Bull. Am. Astron. Soc. 14, 747.

Burns, J.A., Showalter, M.R., Cuzzi, J.N., Durisen, R.H., 1983. Saturn's electrostatic discharges: Could lightning be the cause? Icarus 54, 280–295.

Connerney, J.E.P., Waite, J.H., 1984. New model of Saturn's ionosphere with an influx of water from the rings. Nature 312, 136–138.

Desch, M.D., Fischer, G., Kaiser, M.L., Farrell, W.M., Kurth, W.S., Gurnett, D.A., Zarka, P., Lecacheux, A., Porco, C., Ingersoll, A., Dyudina, U., 2006. Cassini RPWS and imaging observations of Saturn lightning. In: Rucker, H.O., Kurth, W.S., Mann, G. (Eds.), In: Planetary Radio Emissions, vol. VI. Austrian Academy of Sciences Press, Vienna, pp. 103–110.

Dyudina, U.A., IngersollA.P., Shawn, P.E., Porco, C.C., Fischer, G., Kurth, W.S, Desch, M.D., Del Genio, A., Barbara, J., Ferrier, J., 2007. Lightning storms on Saturn observed by Cassini ISS and RPWS in the years 2004–2006. Icarus 190, 545–555.

Esposito, L.W., Cuzzi, J.N., Holberg, J.B., Marouf, E.A., Tyler, G.L., Porco, C.C., 1984. Saturn's rings: Structure, dynamics, and particle properties. In: Gehrels, T., Matthews, M.S. (Eds.), Saturn. Univ. of Arizona Press, Tuscon, pp. 463–545.

Evans, D.R., Warwick, J.W., Pearce, J.B., Carr, T.D., Schauble, J.J., 1981. Impulsive radio discharges near Saturn. Nature 292, 716–718.

Evans, D.R., Romig, J.H., Hord, C.W., Simmons, K.E., Warwick, J.W., Lane, A.L., 1982. The source of Saturn electrostatic discharges. Nature 299, 236–237.

Evans, D.R., Romig, J.H., Warwick, J.W., 1983. Saturn's electrostatic discharges: Properties and theoretical considerations. Icarus 54, 267–279.

Fischer, G., Desch, M.D., Zarka, P., Kaiser, M.L., Gurnett, D.A., Kurth, W.S., Macher, W., Rucker, H.O., Lecacheux, A., Farrell, W.M., Cecconi, B., 2006. Saturn lightning recorded by Cassini/RPWS in 2004. Icarus 183, 135–152.

Giampieri, G., Dougherty, M.K., Smith, E.J., Russell, C.T., 2006. A regular period for Saturn's magnetic field that may track its internal rotation. Nature 441, 62–64, doi:10.1038/nature04750.

Gurnett, D.A., Kurth, W.S., Kirchner, D.L., Hospodarsky, G.B., Averkamp, T.F., Zarka, P., Lecacheux, A., Manning, R., Roux, A., Canu, P., Cornilleau-Wehrlin, N., Galopeau, P., Meyer, A., Boström, R., Gustafsson, G., Wahlund, J.-E., Aahlen, L., Rucker, H.O., Ladreiter, H.P., Macher, W., Woolliscroft, L.J.C., Alleyne, H., Kaiser, M.L., Desch, M.D., Farrell, W.M., Harvey, C.C., Louarn, P., Kellogg, P.J., Goetz, K., Pedersen, A., 2004. The Cassini Radio and Plasma Wave Science investigation. Space Sci. Rev. 114, 395–463.

Gurnett, D.A., Kurth, W.S., Hospodarsky, G.B., Persoon, A.M., Averkamp, T.F., Cecconi, B., Lecacheux, A., Zarka, P., Canu, P., Cornilleau-Wehrlin, N., Galopeau, P., Roux, A., Harvey, C., Louarn, P., Boström, R., Gustafsson, G., Wahlund, J.-E., Desch, M.D., Farrell, W.M., Kaiser, M.L., Goetz, K., Kellogg, P.J., Fischer, G., Ladreiter, H.-P., Rucker, H.O., Alleyne, H., Pedersen, A., 2005. Radio and plasma wave observations at Saturn from Cassini's approach and first orbit. Science 307, 1255–1259.

Hueso, R., Sánchez-Lavega, A., 2004. A three-dimensional model of moist convection for the giant planets. II. Saturn's water and ammonia moist convective storms. Icarus 172, 255–271.

Kaiser, M.L., Connerney, J.E.P., Desch, M.D., 1983. Atmospheric storm explanation of saturnian electrostatic discharges. Nature 303, 50–53.

Kaiser, M.L., Desch, M.D., Connerney, J.E.P., 1984. Saturn's ionosphere: Inferred electron densities. J. Geophys. Res. 89 (A4), 2371–2376.

Lindal, G.F., Sweetnam, D.N., Eshleman, V.R., 1985. The atmosphere of Saturn: An analysis of the Voyager radio occultation measurements. Astron. J. 90, 1136–1146.

Majeed, T., McConnell, J.C., 1996. Voyager electron density measurements on Saturn: Analysis with a time dependent ionospheric model. J. Geophys. Res. 101 (E3), 7589–7598.

Mendillo, M., Moore, L., Clarke, J., Mueller-Wodarg, I., Kurth, W.S., Kaiser, M.L., 2005. Effects of ring shadowing on the detection of electrostatic discharges at Saturn. Geophys. Res. Lett. 32, doi:10.1029/2004GL021934. L05107.

Mendis, D.A., Hill, J.R., Ip, W.-H., Goertz, C.K., Grün, E., 1984. Electrodynamic processes in the ring system of Saturn. In: Gehrels, T., Matthews, M.S. (Eds.), Saturn. Univ. of Arizona Press, Tuscon, pp. 546–589.

Mitchell, C.J., Horányi, M., Havnes, O., Porco, C.C., 2006. Saturn's spokes: Lost and found. Science 311, 1587–1589. 5767.

Moore, L.E., Mendillo, M., Müller-Wodarg, I.C.F., Murr, D.L., 2004. Modeling of global variations and ring shadowing in Saturn's ionosphere. Icarus 172, 503–520.

Nagy, A.F., Kliore, A.J., Marouf, E., French, R., Flasar, M., Rappaport, N.J., Anabtawi, A., Asmar, S.W., Johnston, D., Barbinis, E., Goltz, G., Fleischman, D., 2006. First results from the ionospheric radio occultations of Saturn by the Cassini spacecraft. J. Geophys. Res. 111, doi:10.1029/2005JA011519. A6. A06310.

Porco, C.C., Baker, E., Barbara, J., Beurle, K., Brahic, A., Burns, J.A., Charnoz, S., Cooper, N., Dawson, D.D., Del Genio, A.D., Denk, T., Dones, L., Dyudina, U., Evans, M.W., Giese, B., Grazier, K., Helfenstein, P., Ingersoll, A.P., Jacobson, R.A., Johnson, T.V., McEwen, A., Murray, C.D., Neukum, G., Owen, W.M., Perry, J., Roatsch, T., Spitale, J., Squyres, S., Thomas, P., Tiscareno, M., Turtle, E., Vasavada, A.R., Ververka, J., Wagner, R., West, R., 2005. Cassini imaging science: Initial results on Saturn's atmosphere. Science 307, 1243–1247.

Rakov, V.A., Uman, M.A., 2003. Lightning, Physics and Effects. Cambridge Univ. Press, Cambridge.

Warwick, J.W., Pearce, J.B., Evans, D.R., Carr, T.D., Schauble, J.J., Alexander, J.K., Kaiser, M.L., Desch, M.D., Pedersen, B.M., Lecacheux, A., Daigne, G., Boischot, A., Barrow, C.W., 1981. Planetary radio astronomy observations from Voyager 1 near Saturn. Science 212, 239–243.

Warwick, J.W., Evans, D.R., Romig, J.H., Alexander, J.K., Desch, M.D., Kaiser, M.L., Aubier, M.G., Leblanc, Y., Lecacheux, A., Pedersen, B.M., 1982. Planetary radio astronomy observations from Voyager 2 near Saturn. Science 215, 582–587.

Warwick, J.W., Romig, J.H., Evans, D.R., 1983. Electrostatic discharges in Saturn's B-ring. Adv. Space Res. 3 (3), 105–110.

Weinheimer, A.J., Few Jr., A.A., 1982. The spokes in Saturn's rings: A critical evaluation of possible electrical processes. Geophys. Res. Lett. 9 (10), 1139–1142.

Westphal, J.A., Baum, W.A., Ingersoll, A.P., Barnet, C.D., De Jong, E.M., Danielson, G.E., Caldwell, J., 1992. Hubble Space Telescope observations of the 1990 equatorial disturbance on Saturn: Images, albedos, and limb darkening. Icarus 100, 485–498.

Zarka, P., 1985a. Directivity of Saturn electrostatic discharges and ionospheric implications. Icarus 61, 508–520.

Zarka, P., 1985b. Saturn electrostatic discharges characteristics, comparison to planetary lightning and importance in the study of Saturn's ionosphere. In: Rucker, H.O., Bauer, S.J. (Eds.), Planetary Radio Emission I. Austrian Academy of Sciences Press, Vienna, pp. 161–182.

Zarka, P., Pedersen, B.M., 1983. Statistical study of saturn electrostatic discharges. J. Geophys. Res. 88 (A11), 9007–9018.

Zarka, P., Cecconi, B., Denis, L., Farrell, W.M., Fischer, G., Hospodarsky, G.B., Kaiser, M.L., Kurth, W.S., 2006. Physical properties and detection of Saturn's radio lightning. In: Rucker, H.O., Kurth, W.S., Mann, G. (Eds.), Planetary Radio Emissions, vol. VI. Austrian Academy of Sciences Press, Vienna, pp. 111–122.